A Real-Time Simulator Framework for Marine Power Plants with Weak Power Grids

Stian Skjong[a,*], Eilif Pedersen[a]

[a]*Norwegian University of Science and Technology (NTNU)*
Department of Marine Technology

Abstract

This work takes aim at presenting a generic real-time simulation framework for marine power plants with weak power grids, containing transient functionalities such as starting and stopping of arbitrary generators, and phase synchronization. The generator models used in the power plant are hybrid causality models, meaning that they have the ability to switch between causality orientations, between voltage and current. These models facilitate real-time simulations as long as they are solved properly, as will be discussed in this article. Much is devoted to numerical stability, model robustness and power plant control, e.g. rms voltage control, engine speed control, active- and reactive power sharing control and phase synchronization control. Some focus is also given to overall power plant control structure. A case study of a marine power plant including two generators and a fluctuating- and noisy power consumption is presented and analysed, and illustrates the advantages of the proposed framework as well as giving a good foundation for future works.

Keywords: Weak power grid, real-time power plant framework, marine system, hybrid generator modeling, numerical stability, power plant control

1. Introduction

To date, diesel electric propulsion is the most preferred solution for propulsion generation for marine vessels with a relatively large change in load conditions on a daily basis [1]. This is mostly due to its flexibility and, in general, low emissions [2], even though conversion losses may become quite significant. For a marine vessel all systems that produce electrical power constitute the power plant. Different diesel engine and generator configurations, here referred to as *gensets*, can be used in a marine power plant, depending on the criteria set by the ship-owner and the classification authorities. One such configuration is shown in Figure 1 where two gensets constitute the marine power plant for a vessel equipped with two azimuth thrusters placed at the stern and one tunnel thruster in the bow. For reference, this thruster configuration was studied in [3] with respect to optimal thrust allocation control. Such a marine power plant is often tailored for each marine vessel

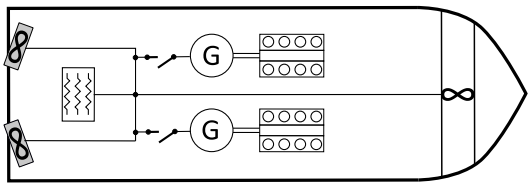

Figure 1: Marine vessel equipped with two gensets, two azimuths and one tunnel thruster, in addition to auxiliary loads such as hotel loads

*Corresponding author
Email addresses: stian.skjong@ntnu.no (Stian Skjong), eilif.pedersen@ntnu.no (Eilif Pedersen)

and a mathematical model of the power plant is a good tool in the design process, enabling simulations of various load conditions, due to different vessel operations. One challenge when it comes to marine power plant modeling is proper control, at least if transient power plant operations are considered, e.g. a constantly changing power demand causing starting and stopping of gensets, and synchronization of gensets when being activated. A marine power plant model that facilitate such studies is the main topic presented in this article.

A diesel-electric marine power plant consists in general of diesel engines and electrical machineries [4], such as generators and electrical motors, which on a component basis have been studied thoroughly in the literature. In [5, 6], a two-axis bond graph model representing synchronous electrical machines is presented and studied. This model, given in the $(d, q, 0)$-reference frame, is also thoroughly analysed in [7], where equivalent circuit diagrams are also given, along with different model fidelities and model reduction techniques. Such model reductions are also studied in [8, 9]. In [7], stability and control of such systems are treated as well, and in [10] the sensitivity of eigenvalues is studied and in [11] the Nyquist stability criterion is used to assure stability in DC power systems. When it comes to overall power plant control, functionalities for synchronizing gensets and for load sharing are important. In [12], active synchronizing control of a microgrid is proposed and studied, while in [13], load sharing control is developed based on droop control and average power control.

Power grids in marine power plants are often characterized as weak, as opposed to onshore ones, which means that in practice, a large power peak in the power grid may change the rms voltage. This is because capacitive effects in the power grid itself are small and often negligible. However, often when modeling such weak power grids, a small capacitive effect is added in order to set the power grid voltage, mathematically speaking. This means that all power grid consumers and producers can be modeled with electrical current as the model output and the power grid voltage as model input. Nevertheless, such a small capacitive effect would introduce a small time constant which often stiffens the system and increases the time to solve the total system in a simulation, and is hardly wanted when trying to achieve real-time simulations.

By neglecting the capacitive effect in the power grid model itself the small time constant disappears. However, then the power grid voltage must be set by one of the power grid components. Consequently, in a generic marine power plant model where arbitrary power producers can be active, all power producers should have the possibility to set the power grid voltage, though only one at a time, if no loading model in parallel is implemented for providing the voltage. A model that has the ability to change input and output variable(s) online during a simulation is hereafter referred to as a *hybrid causality model*. Such a model switches between having *integral causality* and *differential causality*. The concept of causality is thoroughly elaborated in [14] and will not be given any particular attention here. The reason for using hybrid causality generator models in this context is because we then always have one component in the marine power plant that can provide the voltage, and hence, no small capacitive effect introducing a small time constant is needed. However, other problems are introduced, such as solving the differential causality part of the model in a stable and fast manner without algebraic loops. This will be given more attention in section 2.4.2.

In the literature, hybrid causality models are also referred to as switched models [15] and hybrid models, in general. In [16], a theory for modeling discontinuities in models is presented, and in general, treats most kinds of hybrid dynamical models, and in [17] it is shown how simulations can be efficiently built from hybrid bond graph models. Generic synchronous generator models, having hybrid causality properties, are presented in [18] but lacks an overall numerical stability discussion, as well as a presentation of a suited power plant control structure and does not have a focus on real-time solvability.

In this work, a hybrid formulation of the well-known synchronous generator model in the $(d, q, 0)$-reference frame, as first presented in [18] in bond graphs, is further studied with respect to numerical stability, power management and control. This, in order to establish a generic model framework for simulating marine power plants with weak power grids

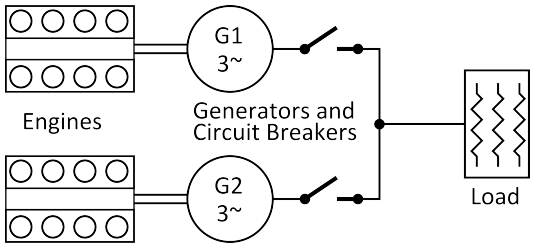

Figure 2: Marine power plant model

suited for transient operations, while maintaining computational efficiency for real-time applications. This is significant because this topic is not overrepresented in the literature and such a generic framework gives great advantages when e.g. studying marine offshore vessels in demanding operations, as in [19], where interactions between the equipment and the power plant is important. If hardware in the simulation loop are included, such as in [20], it is also important that the models can be simulated in real-time. The proposed marine power plant framework also provides generic connections in both the $(d, q, 0)$- and the (a, b, c)-reference frame such that electrical equipment, e.g. azimuth thrusters, can be connected directly. Hence, the proposed power plant framework is a stepping stone for fast solvable total marine vessel simulators, as will be a topic in future works. A marine power plant consisting of two generic three-phased synchronous generator models, stiffly connected through a weak power grid, as shown in Figure 2, will be used as a case study in this work, and will be modeled using bond graph theory [14].

1.1. Outline

In the next section the hybrid causality generator model is presented in detail and analysed with respect to numerical stability when using the Euler integration method. Also, additional models such as auxiliary diesel engines and circuit breakers are presented. In section 3 simple control systems and strategies needed for running a marine power plant is presented. A case study of a marine power plant including two gensets are studied and simulated in section 4. Lastly, a conclusion is made in section 5.

2. Hybrid Generator Modeling

The hybrid generator models to be used are given in the $(d, q, 0)$-reference frame as in [18]. To keep it generic, as well as the ability to display simulation results in the (a, b, c)-reference frame, these models should have the ability to connect to the (a, b, c)-reference frame, which means that a power conservative transformation between the two reference frames is of interest.

2.1. Reference Frame Transformation

According to [5, 21], the $(d, q, 0)$-reference frame is related to the (a, b, c)-reference frame through the phase angle θ such that

$$\begin{aligned} \boldsymbol{u}_{d,q,0} &= A(\theta)\boldsymbol{u}_{a,b,c} \\ \boldsymbol{i}_{d,q,0} &= A^{-1}(\theta)\boldsymbol{i}_{a,b,c} \end{aligned} \tag{1}$$

where $\boldsymbol{u}_{i,j,k} = [u_i, u_j, u_k]^T$, $\boldsymbol{i}_{i,j,k} = [i_i, i_j, i_k]^T$, and

$$A(\theta) = \sqrt{\frac{2}{3}} \begin{bmatrix} \cos(\theta) & \cos\left(\theta - \frac{2}{3}\pi\right) & \cos\left(\theta - \frac{4}{3}\pi\right) \\ -\sin(\theta) & -\sin\left(\theta - \frac{2}{3}\pi\right) & -\sin\left(\theta - \frac{4}{3}\pi\right) \\ \frac{1}{\sqrt{2}} & \frac{1}{\sqrt{2}} & \frac{1}{\sqrt{2}} \end{bmatrix} \tag{2}$$

is a power-conserving transformation matrix. The phase angle θ is defined as

$$\theta = \int_0^t f_{PG} 2\pi dt \tag{3}$$

Here, f_{PG} is the power grid frequency. In order for this transformation to be power conservative, it follows directly that $A(\theta)^{-1} = A(\theta)^T$ [7]. Here, it is assumed that $u_0 = 0$. In other words, u_d, u_q and f_{PG} is a representative set of variables for u_a, u_b and u_c.

2.2. Generator Model with Current as Output

The dynamics of a generator with current as output can be expressed according to [18] as

$$\dot{\boldsymbol{\psi}} = -\omega_m \boldsymbol{D}\boldsymbol{\psi} - \boldsymbol{R}\boldsymbol{i} + \boldsymbol{E}\boldsymbol{u}_{\boldsymbol{d},\boldsymbol{q}} + \boldsymbol{b}u_f \tag{4a}$$

$$\boldsymbol{i} = \boldsymbol{L}^{-1}\boldsymbol{\psi} \tag{4b}$$

where ω_m is the engine speed, $\boldsymbol{\psi} = [\psi_d, \psi_q, \psi_f, \psi_D, \psi_Q]^T$ is the magnetic fluxes for

d, q, the field and the damping in d and q, respectively, $\boldsymbol{i} = [i_d, i_q, i_f, i_D, i_Q]^T$ is the current vector, u_f is the field voltage that controls the generator and

$$\boldsymbol{D} = \begin{bmatrix} 0 & -n_p & 0 & 0 & 0 \\ n_p & 0 & 0 & 0 & 0 \\ 0 & 0 & 0 & 0 & 0 \\ 0 & 0 & 0 & 0 & 0 \\ 0 & 0 & 0 & 0 & 0 \end{bmatrix}, \ \boldsymbol{E} = \begin{bmatrix} 1 & 0 \\ 0 & 1 \\ 0 & 0 \\ 0 & 0 \\ 0 & 0 \end{bmatrix}$$

$$\boldsymbol{R} = \begin{bmatrix} R_d & 0 & 0 & 0 & 0 \\ 0 & R_q & 0 & 0 & 0 \\ 0 & 0 & R_f & 0 & 0 \\ 0 & 0 & 0 & R_D & 0 \\ 0 & 0 & 0 & 0 & R_Q \end{bmatrix}, \ \boldsymbol{b} = \begin{bmatrix} 0 \\ 0 \\ 1 \\ 0 \\ 0 \end{bmatrix} \quad (5)$$

$$\boldsymbol{L} = \begin{bmatrix} L_d & 0 & L_{df} & L_{dD} & 0 \\ 0 & L_q & 0 & 0 & L_{qQ} \\ L_{df} & 0 & L_f & L_{fD} & 0 \\ L_{dD} & 0 & L_{fD} & L_D & 0 \\ 0 & L_{qQ} & 0 & 0 & L_Q \end{bmatrix}$$

Here, $\boldsymbol{R}$ is the internal resistance matrix, $\boldsymbol{L}$ is the inductance matrix and n_p is the number of pole pairs in the generator. The electromagnetic torque feedback to the engine is given as

$$T_e = (\psi_d i_q - \psi_q i_d) n_p \quad (6)$$

2.3. Generator Model with Voltage as Output

The equations in (4) and (5) show that the differential equations are coupled, which means that the entire system of differential equations must be altered in order to obtain voltage as output in the generator model. This means that u_d and u_q should be calculated from ψ_d, ψ_q, i_f, i_D and i_Q. Thus, two of the differential equations in (4) are given differential causality, meaning that integration is replaced by differentiation when solving the model. By separating these two equations from the differential equations, they may be written as

$$\boldsymbol{u}_{d,q} = \dot{\boldsymbol{\psi}}_{d,q} + \omega_m \boldsymbol{D}_{d,q} \boldsymbol{\psi}_{d,q} + \boldsymbol{R}_{d,q} \boldsymbol{i}_{d,q} \quad (7)$$

where $\boldsymbol{u}_{d,q} = [u_d, u_q]^T$, $\boldsymbol{\psi}_{d,q} = [\psi_d, \psi_q]^T$, $\boldsymbol{i}_{d,q} = [i_d, i_q]^T$ and

$$\boldsymbol{R}_{d,q} = \begin{bmatrix} R_d & 0 \\ 0 & R_q \end{bmatrix}, \ \boldsymbol{D}_{d,q} = \begin{bmatrix} 0 & -n_p \\ n_p & 0 \end{bmatrix} \quad (8)$$

It is then possible to rearrange (4b) such that

$$\begin{bmatrix} \boldsymbol{\psi}_{d,q} \\ \boldsymbol{i}_{f,D,Q} \end{bmatrix} = \boldsymbol{Z} \begin{bmatrix} \boldsymbol{i}_{d,q} \\ \boldsymbol{\psi}_{f,D,Q} \end{bmatrix} \quad (9)$$

which means that $\boldsymbol{\psi}_{d,q}$ can be calculated from (9), differentiated and inserted into (7) to find $\boldsymbol{u}_{d,q}$. The current vector $\boldsymbol{i}_{f,D,Q}$ is found by first obtaining $\dot{\boldsymbol{\psi}}_{f,D,Q}$ from a reduced version of (4), integrating and inserting into (9). Note that $\boldsymbol{Z}$ is a rearranged version of $\boldsymbol{L}$, and can be found by solving (4b) with respect to $\boldsymbol{\psi}_{d,q}$ and $\boldsymbol{i}_{f,D,Q}$.

The electromagnetic torque given in feedback to the engine driving the generator is still as given in (6). Note that these two sets of equations describing the generator dynamics do not include saturation of the magnetic fluxes. This can be added by including a saturation function that saturates the magnetic fluxes after integration.

2.4. Hybrid Causality Model

The two different causality representations of the generator model can be put together to form the hybrid causality generator model, as done in [18]. Since causality switching happens in discrete time events, the power during switching should be conserved. For this reason, the input and the output from the old causality configuration must be inherited and used as initial conditions in the new causality configuration.

2.4.1. Discrete Switches

In addition to inheritance of variables, different switches are needed. The model input and output ports must be controlled by switches that routes signals from one model causality to another to make sure that the connectivity specifications in the model environment are not violated. Such switches are also needed to model the circuit breakers that connect the generators to the power grid. In [22] a design for such switches are proposed and derived using bond graph theory.

Here, only one type of switch is needed, namely a *flow switch*. This switch is often referred to as a switched 0-junction, an **0s**-junction. This name comes from its mnemonic symbolic representation in

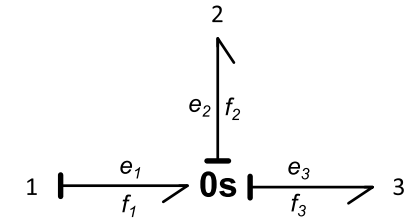

(a) Bond graph representation.

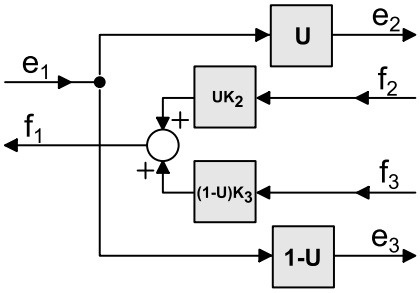

(b) Block diagram representation.

Figure 3: Switched 0-junction.

bond graph theory. The switched 0-junction is shown in Figure 3, both in bond graphs and block diagrams.

The equations in the switched 0-junction are given as

$$\begin{aligned} e_1 =& Ue_2 + (1-U)e_3 \\ f_1 =& UK_2f_2 + (1-U)K_3f_3 \end{aligned} \tag{10}$$

where

$$U = \begin{cases} 1, & \text{when port 2 is active} \\ 0, & \text{when port 3 is active} \end{cases} \tag{11}$$

and

$$K_2, K_3 = \begin{cases} 1, & \text{for addition} \\ -1, & \text{for subtraction} \end{cases} \tag{12}$$

2.4.2. Numerical Differentiation using Filter

In comparison to the current causality model that has five integral causalities, the voltage causality model has two differential causalities and three integral causalities. It is always preferable to have integral causality due to the use of explicit solvers, and to avoid the direct differentiation of $\boldsymbol{\psi}_{d,q}$. In [6], it is proposed to differentiate $\boldsymbol{\psi}_{d,q}$ by using a low-pass filter with derivative effect given as

$$H(s) = \frac{s}{1+Ts} \tag{13}$$

where the time constant T is chosen small, typically 0.001 s. This transfer function changes the differential causalities to integral causalities when solved in the time plane, which may enable explicit fixed-step solvers such as the Euler integration method, as used here. Note that the poles and the zeros of the dynamical system also set requirements for which solver to use. As it turns out, the transfer function-based differentiation also has a positive effect on solvers due to the low-pass filtering effect, and will filter out high frequent oscillations due to numerical errors, having negligible effects on the simulation results when tuned properly.

2.4.3. Numerical Stability and Solver Time Step

The generator parameters used in this paper are given in Table 5 in the Appendix. By assuming a constant generator speed corresponding to 60 Hz in power grid frequency, corresponding to an engine speed of 720 rpm when having five pole pairs, open-loop pole-zero plots can be constructed for the two generator state space models given in sections 2.2 and 2.3. The pole-zero plots for the generator models with voltage output and current output are given in Figures 4 and 5, respectively.

As can be seen in Figure 4 the generator model with voltage outputs has the poles and the zeros inside the stability region for the Euler integration method when $i_d = i_q = 0$ and $\Delta t \leq 0.002$ s, where Δt is the solver time step. This indicates that the Euler integration method can be used to solve the model as long as the model environment does not introduce poles and zeros that are outside the stability region. The reasons for using the Euler integration method here are that it is fast when a reasonable step size can be used, and since it is a fixed-step solver it is easy to control in hybrid model simulations, where integrator resets and state inheritances are important. Also, when the system is proven stable with the Euler integration method, the results when using Runge-Kutta integration methods are also stable [23]. Note that

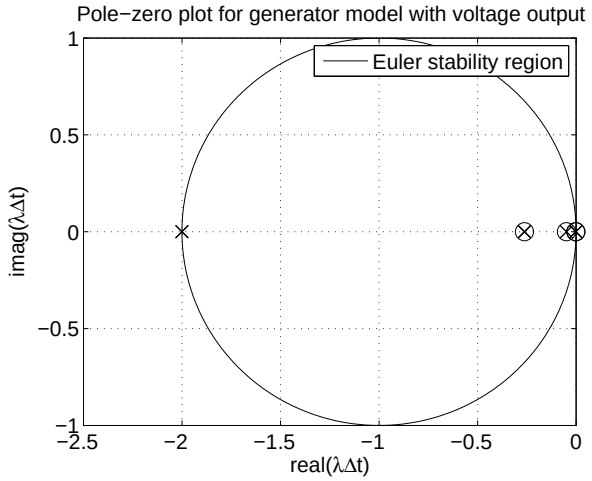

Figure 4: Only internal generator load ($i_d = i_q = 0$)

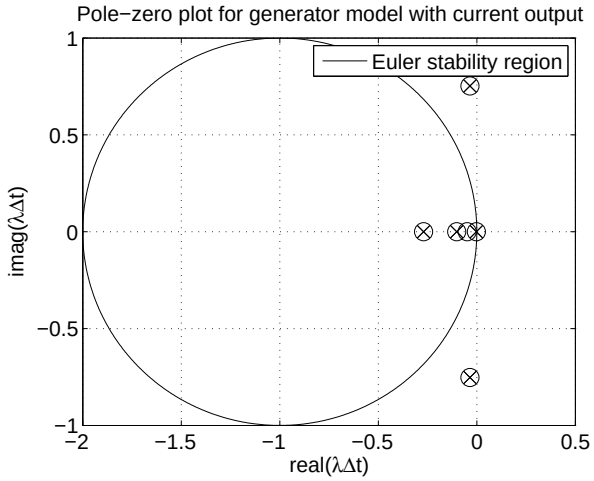

Figure 5: Only internal generator load ($i_d = i_q = 0$)

implicit numerical solvers can be used as well, but is harder to control when it comes to integrator resets and state inheritances, and hence, more implementation work must be expected. The same goes for variable step-sizes where zero-crossing detection must be implemented in order to properly handle discrete events.

Figure 5 shows that by using the same time step, $\Delta t = 0.002\,\mathrm{s}$, the Euler integration method will fail to converge to any solution due to the poles and zeros outside the stability region. As a matter of fact, the time step must be reduced by a factor of approximately 10 in order to stabilize the zero input case, and to approximately $\Delta t = 5 \cdot 10^{-12}\,\mathrm{s}$ if an open circuit load of $R = 10^8$ is to be considered. This is without taking the model environment into consideration. If even possible, such a low time step would result in a long simulation time when solving the system, which is not desired, especially when it comes to achieving real-time simulations. Nonetheless, this problem may be solved by choosing the simulation setup or through proper pole-zero cancelling control designs, with the first mentioned treated in this paper.

By recognizing that the complex conjugated poles and zeros are dependent on the $[i_d, u_d]$- and $[i_q, u_q]$-pairs, the model will be stable when solved by the Euler integration method if u_d and u_q are stabilized by the generator model environment. Since the poles in the generator model with voltage output are almost unaffected by large open-circuit resistances, the voltage output causality model can be used to stabilize the model with current output causality. In other words, the generator model with current as output should only be used in parallel with a generator model that has voltage output causality, because if the generator with voltage outputs is stable, the voltage inputs u_d and u_q to the generator model with current output causality will also be stable, and thus, stabilize the entire generator model. This can also be shown in Figure 6.

It can be seen in Figure 6(a) that when the time step is reduced to $\Delta t = 0.00099\,\mathrm{s}$, the two causality models connected together are stable using the Euler integration method and the parameters given in Table 5 in the Appendix. The two complex conjugated poles and zeros in the figure are dependent on the time constant chosen in the transfer function given in (13). This means that when the time step is chosen, such that $\Delta t < T$ and the controllers and model environment are stable, the whole power plant model would be stable for all reasonable power plant

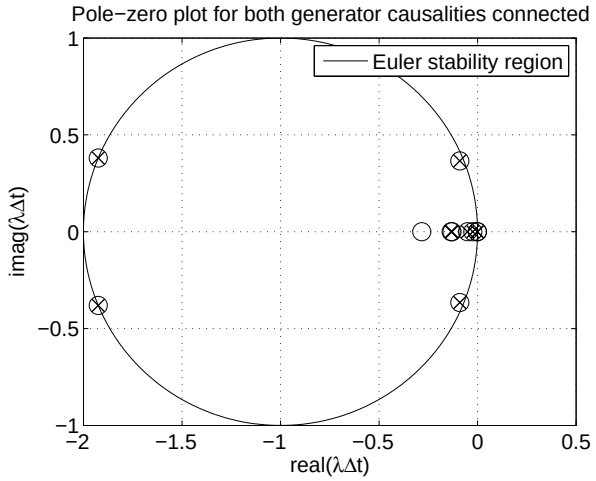

(a) Only internal generator load ($i_d = i_q = 0$)

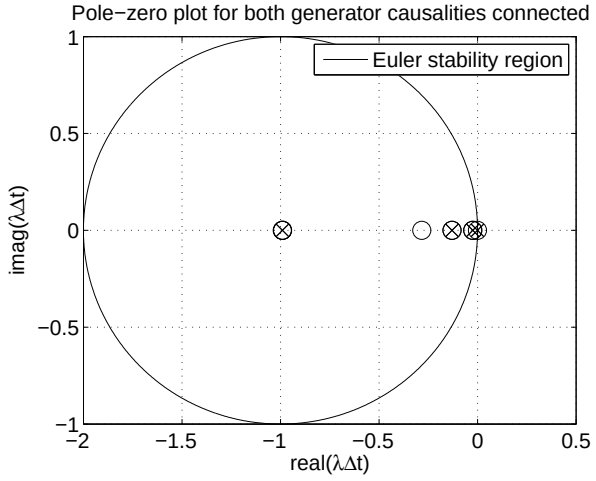

(b) Open circuit load, $R = 1 \cdot 10^8 \Omega$

Figure 6: Euler stability regions for both causality models connected, $\Delta t = 0.00099\,\mathrm{s}$

loads. As a matter of fact, by increasing the power grid load more damping is added and the complex conjugated poles shown in Figure 6 will become real and be moved towards the origin, as shown in Figure 6(b). This means a larger time step can be used when running the generators against a power grid consumer, and indicates that running the generators in open circuit mode would be the operation that requires the smallest time steps. Hence, when ramping up a generator and synchronizing the generator, a model with voltage output should be used, and when another generator sets the grid voltages the generator model should switch causality when the circuit breaker is closed.

It is also important that the solver time step size is chosen such that it is possible to capture the true dynamic characteristics of both the generator models and the power grid load. According to [24] the proper time-step duration must be determined to accurately represent the system frequency response up to the fastest transient of interest. For example, if the power grid load is modeled in the (a, b, c)-reference frame, having a frequency of 60 Hz, the time step size must be set such that $\Delta t \leq \frac{1}{120}\,\mathrm{s}$ in order to catch the main characteristics of the alternating currents and voltages according to the Nyquist sampling criterion [25]. In addition, the solver time step size must also be set low enough to replicate the loading characteristics themselves. However, it is believed that these characteristics will have a lower frequency than the power grid frequency, such as the meeting frequency between the wave loads and the vessel when considering a vessel in transit. Also, when studying higher order harmonic distortions in the power grid, the solver time step size must be adjusted correspondingly.

2.4.4. Implementation and Phase Angle

The resulting hybrid generator model is shown in a bond graph implementation in Figure 7. Note that $\hat{\theta}$ given in the figure is not necessary equal to θ. Since the $(d, q, 0)$-reference frame is more or less a DC representation of the actual AC system, the phase angle between the generators must be included before connecting the generators to a common power grid in order to enable phase synchronization and power sharing, which will be elaborated later on.

In general, the phase transformation is given as

$$\boldsymbol{u}_{PG} = \boldsymbol{S}(\phi)\boldsymbol{u}_G \tag{14}$$

for a generator with voltage outputs, the lead generator, where $\boldsymbol{u}_{PG}$ is the d and q power grid voltages, $\boldsymbol{u}_G$ is the d and q generator voltages and

$$\boldsymbol{S}(\phi) = \begin{bmatrix} \cos(\phi) & -\sin(\phi) \\ \sin(\phi) & \cos(\phi) \end{bmatrix} \tag{15}$$

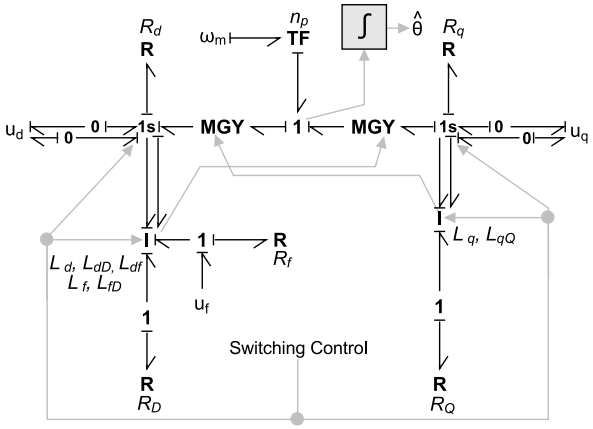

Figure 7: Bond graph model of hybrid generator model

where ϕ is the phase difference between the leading generator and the present generator,

$$\phi = \int_0^t (\Delta\omega_m)dt = \hat{\theta}_l - \hat{\theta} \tag{16}$$

Here, $\Delta\omega_m = \omega_{m,l} - \omega_m$ is the difference in motor velocity between the two engine speeds driving the generators and $\omega_{m,l}$ and $\hat{\theta}_l$ is the speed and phase angle of the leading generator, respectively. This difference in phase angles is usually only calculated when generators are active, meaning that they are either preparing for synchronization or already connected to the power grid, which also means that an integrator reset algorithm should be implemented.

The phase angle used in the transformation between the (a, b, c)- and $(d, q, 0)$ reference frame, given in (2), must then account for ϕ. Hence, the phase angle for a leading generator when only two generators are active is then given as

$$\theta_{Gl} = 2\pi \int_0^t f_{G,l}dt - \phi \tag{17}$$

where f_{Gl} is the lead generator frequency. The phase angle can be found similarly for the other generator,

$$\theta_{G2} = 2\pi \int_0^t f_G dt + \phi \tag{18}$$

where ϕ is defined as in (16).

Table 1: Phase transformations.

	Voltage Output	**Current Output**
Voltage	$\boldsymbol{u}_{PG} = \boldsymbol{S}(\phi)\boldsymbol{u}_G$	$\boldsymbol{u}_G = \boldsymbol{S}^{-1}(\phi)\boldsymbol{u}_{PG}$
Current	$\boldsymbol{i}_G = \boldsymbol{S}^{-1}(\phi)\boldsymbol{i}_{PG}$	$\boldsymbol{i}_{PG} = \boldsymbol{S}(\phi)\boldsymbol{i}_G$

The different transformations between the power grid and the two causality models are shown in Table 1.

2.5. Additional Models needed for Simulation

To be able to set up a simulation testing for the generators, additional models must be included, e.g. circuit breakers, power grids and engine models, in addition to controllers and a power management system.

2.5.1. Circuit Breakers and Power Grid Model

Multiple switched 0-junctions are used to model the circuit breakers and the power grid. In the circuit breaker, model port 1 of the switched 0-junction is connected to the generator model output, port 2 is connected to an open circuit load and port 3 is connected to the power grid. Note that several switched 0-junctions are needed in one circuit breaker model since the generator model has a total of four inputs and outputs, due to the two causality configurations connected to the grid. These circuit breakers are connected to each other and to the consumer models in the power grid through another set of switched 0-junctions, due to the causality switching in the generator models. The total model of a circuit breaker is shown in Figure 8 in bond graphs. Note that each switched 0-junction is also given a control signal, U, as in (10), and that additional switched 0-junctions are needed to connect several gensets to a common power grid.

2.5.2. Simplified Engine Model

The auxiliary engine models used to drive the generator models are based on simple equations given in [26]. The effective engine power is given as

$$P_e = \dot{m}_f h_n \eta = T_m \omega_m \tag{19}$$

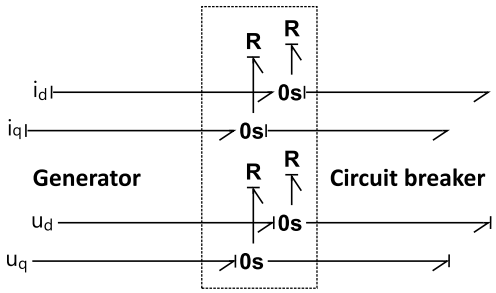

Figure 8: Bond graph model of circuit breaker

where $\dot{m}_f$ is the fuel flow rate, h_n is the lower heating value of the fuel, η is the effective thermal efficiency, T_m is the torque and ω_m is the engine speed. By rearranging the equation, the mean torque generated by the combustion process can be expressed as

$$T_m = \frac{\dot{m}_f h_n \eta}{\omega_m} \tag{20}$$

The fuel flow rate may be expressed as

$$\dot{m}_f = m_{inj} \frac{\omega_m}{2\pi k} \tag{21}$$

where m_{inj} is the amount of fuel injected per cycle and k is a parameter distinguishing two-stroke engines from four-stroke engines, $k = 1$ for two-stroke and $k = 2$ for four-stroke. The efficiency can be expressed as

$$\eta = \frac{1}{b_e(P_e) h_n} \tag{22}$$

where $b_e(P_e)$ is the specific fuel consumption as a function of effective engine power, and can be measured for a specific engine given the engine speed. By assuming a four-stroke engine, the torque can then be expressed as

$$T_m = \frac{m_{inj}}{4\pi b_e(P_e)} \tag{23}$$

The set of differential equations representing the auxiliary engine model is then to be given as

$$\dot{\theta}_m = \omega_m \tag{24a}$$

$$\dot{\omega}_m = \frac{1}{J_m + J_G} \left(T_m - b_f \omega_m - b_b \omega_m^n - T_e \right) \tag{24b}$$

where θ_m is the engine angle, J_m is the inertia of the engine, J_G is the inertia of the generator, T_e is the electromagnetic torque as given in (6), b_f is a friction parameter, b_b is the braking effect when the engine is choked, which happens when no fuel is injected into the engine due to the pumping work and n is a small number, typically ~ 0.1. Note that $b_b := 0$ when $m_{inj} \neq 0$. To make the transition smooth, the value of b_b is low-pass filtered, having a small time constant before being used in (24).

2.5.3. Power Grid Consumer

The power grid consumer has the role of loading the power grid. This can be a set of thrusters, as well as the auxiliary systems needed to power the ship. Here, it is assumed that the active- and reactive power consumption can be set and based on the power grid voltage, as current can be given in feedback. The active power and reactive power in the $(d, q, 0)$-reference frame are given as

$$P = \boldsymbol{u}_{d,q}^T \begin{bmatrix} 1 & 0 \\ 0 & 1 \end{bmatrix} \boldsymbol{i}_{d,q} \tag{25a}$$

$$Q = \boldsymbol{u}_{d,q}^T \begin{bmatrix} 0 & -1 \\ 1 & 0 \end{bmatrix} \boldsymbol{i}_{d,q}, \tag{25b}$$

respectively. Note that reactive power is related to impedance in the (a, b, c)-reference frame. By solving (25a) and (25b) with respect to $\boldsymbol{i}_{d,q}$ the current given in feedback is given as

$$\boldsymbol{i}_{d,q} = \frac{1}{||\boldsymbol{u}_{d,q}||_2^2} \begin{bmatrix} P u_d + Q u_q \\ P u_q - Q u_d \end{bmatrix} \tag{26}$$

where

$$||\boldsymbol{u}_{d,q}||_2^2 = u_d^2 + u_q^2 \tag{27}$$

is the square of the $\mathcal{L}_2$-norm. To avoid dividing by zero at the start of the simulation, a small number is added to the denominator. Also, two low-pass filters are used to filter the input voltages in order to avoid algebraic loops.

2.5.4. Power Management System, PMS

Power management systems are in reality quite complex [27]. In this paper, the PMS is treated as a collection of controllers with some automated decision-making functionalities. This will be highlighted in section 3.3.

3. Power Plant Control

In general, systems that produce electric power require proper control dependent on the operation in order to run satisfactory [28]. For generators, proper control of the generator phase synchronization, voltage control and load sharing, or power sharing, are crucial for running the power plant within its limits.

In general, a genset only has two controllable variables, namely the engine speed and the field voltage, which means that more than one objective must be controlled through each controllable variable. In single model systems this is not preferred since it often sacrifices stability or degradation of the control strategies. However, in power plants, a single genset connected to a power grid only has to control the frequency and rms voltage, which can be separately done through the two controllable variables. It is only when two or more gensets are connected that multiple control strategies must be merged into the two control variables. This can be done in a stable manner in such systems due to the stiff coupling between gensets, since the difference in frequency, rms voltage and phase can be indirectly controlled.

In this section, different controllers needed to run the model shown in Figure 2 are presented.

3.1. Automatic Voltage Regulator (AVR) and Reactive Power Sharing

Both the rms voltage and reactive power sharing are controlled through the field voltage, but the reactive power sharing control is only activated when two or more generators are synchronized and connected together.

3.1.1. AVR

The voltage magnitude, or the rms voltage, is regulated in each generator by an automatic voltage regulator (AVR). The AVR regulates the voltage magnitude through the generator field voltage, which sets the magnetic field in the stator. The rms voltage in the $(d, q, 0)$-reference frame for a generator i is given as

$$V_{rms_i} = \sqrt{\frac{2}{3}}||\boldsymbol{u}_{dq,i}||_2 \tag{28}$$

Note that $\boldsymbol{u}_{dq,i}$ is the voltage vector for the active causality model of the generator. There exists many different control laws for AVRs, such as the one presented in [29] with pole assignment self-tuning regulator. Nevertheless, here the rms voltage is controlled by a simple PI-controller, and the controller error for generator i is defined as

$$e_{Vi} = V_{ref} - V_{rms,i} \tag{29}$$

where V_{ref} is the reference rms voltage. Hence, the corresponding controller output u_{Vi} can be expressed as

$$u_{Vi} = K_p^{AVR} e_{Vi} + \frac{K_p^{AVR}}{T_i^{AVR}} \int_0^t e_{Vi} dt \tag{30}$$

where K_p^{AVR} and T_i^{AVR} are the proportional gain and the integral time constant, respectively. In order to avoid commanding an unrealistic field voltage the controller output is saturated before being sent to the generator model. Hence, an integration anti-windup algorithm [30] is implemented in the controller as well.

3.1.2. Reactive Power Sharing

Control of the reactive power is found in the PMS since reactive power sharing control needs measurements from all active generators, which is why it cannot be implemented as local controllers inside each generator. Another reason is that it is only active when two or more generators are active. This means that global power plant surveillance is needed, which is a PMS functionality. Power sharing in general is thoroughly discussed in [31], and only a simple method for controlling the reactive power sharing is presented here.

By assuming that N number of generators are connected to the power grid, the reactive power sharing can be controlled by means of PI-controllers where the error for generator i is defined as

$$e_{Qi} = S_{Qi} Q_{tot} - Q_{Gi} \tag{31}$$

and where $S_{Qi} \in [0, 1]$ is the sharing factor, Q_{Gi} is the reactive power for generator i and

$$Q_{tot} = \sum_{i=1}^{N} Q_{Gi} \tag{32}$$

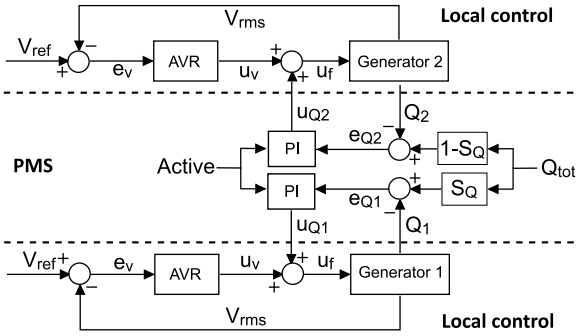

Figure 9: AVR and reactive power sharing, RPS, control structure for two active gensets

is the total reactive power in the power grid, or the reactive power for the power grid load. Hence, the corresponding controller output u_{Qi} can be expressed as

$$u_{Qi} = K_p^Q e_{Qi} + \frac{K_p^Q}{T_i^Q} \int_0^t e_{Qi} dt \tag{33}$$

where K_p^Q and T_i^Q are the proportional gain and the integral time constant, respectively. Note that if equal reactive power sharing is considered, then $S_{Qi} = \frac{1}{N}$. Thus, the total field voltage that is fed to generator i is then given as

$$u_{fi} = u_{Vi} + u_{Qi} \tag{34}$$

Here, only two generators are considered in the power plant, and the controller errors for the reactive power sharing control for the two generators are defined as

$$e_{Q1} = S_Q Q_{tot} - Q_{G1} \tag{35a}$$
$$e_{Q2} = (1 - S_Q) Q_{tot} - Q_{G2} \tag{35b}$$

respectively, where $S_Q \in [0, 1]$ is the sharing factor.

Since the reactive power sharing controllers are only activated when two or more generators are synchronized and connected to the power grid, integrator reset algorithms must also be implemented in the reactive load sharing controllers. The structure of the total rms voltage control system and the reactive power sharing control system is shown in Figure 9 for two active genesets.

3.2. Engine Control, Active Power Sharing and Generator Synchronization

The last control variable is the engine speed driving the generator. In general, the auxiliary engine is to maintain a constant speed that corresponds to the wanted power grid frequency, but also generator synchronization and active power sharing can be done through the engine speed, the last one by means of *droop-control* [13].

3.2.1. Engine Control

The engine speed controller, commonly known as the *engine governor* , is in general complex [32], but is assumed here to be a simple PI-controller that controls the engine speed, such that the power grid frequency is kept more or less constant. The reference engine speed is given as

$$\omega_{ref} = \frac{2\pi f_{PG}}{n_p} \tag{36}$$

In comparison to the field voltage control and the reactive power control, active power sharing control and phase synchronization control are applied to the reference signal before being fed into the PI-controller. The reference fed to the controller is denoted $\omega_{ref,ni}$ for generator i, as will be defined in section 3.2.3, and the controller error can be expressed as

$$e_{\omega_i} = \omega_{ref,ni} - \omega_{mi} \tag{37}$$

where ω_{mi} is the measured engine speed for genset i. Hence the corresponding control output $m_{inj,i}$ can be expressed as

$$m_{inj,i} = K_p^\omega e_{\omega_i} + \frac{K_p^\omega}{T_i^\omega} \int_0^t e_{\omega_i} dt \tag{38}$$

where K_p^ω and K_i^ω are the proportional gain and the integral gain, respectively. Also this control output is saturated in order to give realistic fuel injections to the engine. Hence, an integrator anti-windup algorithm is implemented in the controller as well.

3.2.2. Synchronization Control

In the (a, b, c)-reference frame, the phase synchronization controller makes the phase angles converge

through controlling the engine speed of the generator that is to be synchronized. However, in the $(d, q, 0)$-reference frame, it is enough to make the d voltages converge, since the q voltages will then converge due to the AVR, in order to make the phases converge. This can be shown by setting the criterion

$$u_{al} = u_{ai} \tag{39}$$

where u_{al} and u_{ai} are the a voltages in the (a, b, c)-reference frame for the lead generator and the generator i, which is to be synchronized, respectively. This gives the criterion in the $(d, q, 0)$-reference frame

$$(\cos\theta_i - \cos\theta_l)u_d = (\sin\theta_i - \sin\theta_l)u_q \tag{40}$$

when the d voltages converge. The only solution of (40) for all values of u_d and u_q is $\theta_l = \theta_i$, which means that by making the d voltages converge a solution for $\theta_l = \theta_i$ exists under the restriction given in (40). By also requiring that $u_{bl} = u_{bi}$ and $u_{cl} = u_{ci}$ the only solution left is $\theta_l = \theta_i$ if all the criteria are to be held. This means that by making the difference in the d-voltages converge, the difference in the phase angles will also converge.

The main reason for comparing the voltages instead of the phase angles is because the causality switching requires equal voltages and currents right before and after switching, and due to the risk of numerical deviations when simulating, it is better to compare the voltages directly in the phase synchronization controller. When the phase synchronization controller is active, the control errors for phase synchronization between the lead generator l and generator i can then be given as

$$e_{PSi} = u_{dl} - u_{di}, \tag{41}$$

for the generator i that is to be connected to the grid. Note that the lead generator is defined as one generator that is already connected to the grid. Hence the corresponding control output u_{PSi} can be expressed as

$$\begin{aligned} u_d &= \frac{N_d^{PS}}{T_d^{PS}} \int_0^t u_{dPSi} dt \\ u_{dPSi} &= K_p^{PS} N_d^{PS} e_{PSi} - u_d \\ u_{PSi} &= K_p^{PS} e_{PSi} + u_{dPSi} \end{aligned} \tag{42}$$

where K_p^{PS} and N_d^{PS} and T_d^{PS} are the proportional gain, the derivative gain limitation and the derivative time constant, respectively. Note that u_d and u_{dPSi} are initially set to zero and that the control equations given in (42) should be calculated in the given order. Also in this controller the output is saturated in order not to give too large of deviations in the engine speeds. Hence, an integrator anti-windup algorithm is implemented as well.

3.2.3. Active Power Sharing through Droop Control

Droop control is not a controller in common sense, but more like an algorithm, due to its multiple outputs. The intention with the droop controller is to give the reference signal a small continuous peak, and when gensets get peaks with opposite signs the power sharing is controlled. A negative peak gives a genset more active power, and a positive peak reduces the active power. This means that the amount of power a given generator produces can be adjusted by subtracting a reference power measure from the engine reference speed and adding an actual power measure to the engine reference speed, such that the new engine reference speed for engine i becomes

$$\omega_{ref,ni} = \omega_{ref} + K_{aps}(P_{mi} - P_{ref,i}) \tag{43}$$

where ω_{ref} is the commanded engine reference speed, K_{aps} is a proportional gain, P_{mi} is the measured power and $P_{ref,i}$ is the reference power. Then, if the power is too low, the engine speed will drop so that more load is added to the respective generator. If the power is too high, the opposite occurs.

When using droop control for active power sharing, one can choose to share the load using the load magnitude, or using the loading percentage for each genset. Here, the loading percentage is used. Note that equal power sharing in this context means that each genset has the same loading percentage, though not necessarily an equal load. In order for this to be true, all gensets must be equal.

The engine power fraction used in droop control is defined for engine i as

$$L_{mi} = \frac{T_{mi}\omega_{mi}}{P_{ei,max}} \tag{44}$$

where T_{mi} is the engine torque as defined in (23), ω_{mi} is the engine angular rate and $P_{ei,max}$ is the lowest maximally rated effective power for the engine and the generator. For a power plant with an N number of gensets, the total load fraction is the defined as

$$L_{tot} = \sum_{i=1}^{N} L_{mi} \tag{45}$$

When the droop control is active, the reference power fraction is subtracted from the reference speed and is for generator i given as

$$\omega_{drp1}(i) = K_D S_{Pi} L_{tot} \omega_{ref} \tag{46}$$

where K_D is the droop gain and $S_{Pi} \in [0, 1]$ is the active power-sharing constant. Note that (46) is run through a low-pass filter with filter time constant T_{LP} in order to smooth the signal before being subtracted from ω_{ref}. Also note that $S_{Pi} L_{tot} \leq 1$.

Next, $\omega_{drp2}(i)$ is added to $\omega_{ref} - \omega_{drp1}(i)$ when the droop control is active, and is given as

$$\omega_{drp2}(i) = K_D L_{mi} \omega_{ref} \tag{47}$$

where L_{mi} is the local power fraction defined in (44). $\omega_{drp2}(i)$ is also low-pass filtered in order to smooth the signal. When comparing the expressions for ω_{drp1} and ω_{drp2} to (43), it can be seen that $K_{aps} = K_D \omega_{ref}$, $P_{mi} = L_{mi}$ and $P_{ref,i} = S_{Pi} L_{tot}$. By including the phase synchronization control the PI-controller error for the engine driving generator i is then rewritten as

$$e_{\omega_i} = \omega_{ref} - \omega_{drp1}(i) + \omega_{drp2}(i) - u_{PSi} - \omega_{mi} \tag{48}$$

where u_{PSi} is as defined in section 3.2.2. The PI control law is as given in (38).

Figure 10 shows a graphical representation of the engine speed control, droop control and phase synchronization for genset 1 and genset 2. More advanced load sharing control strategies than the one presented here can also be applied, e.g. as the one presented in [13] where droop control and average power control are combined.

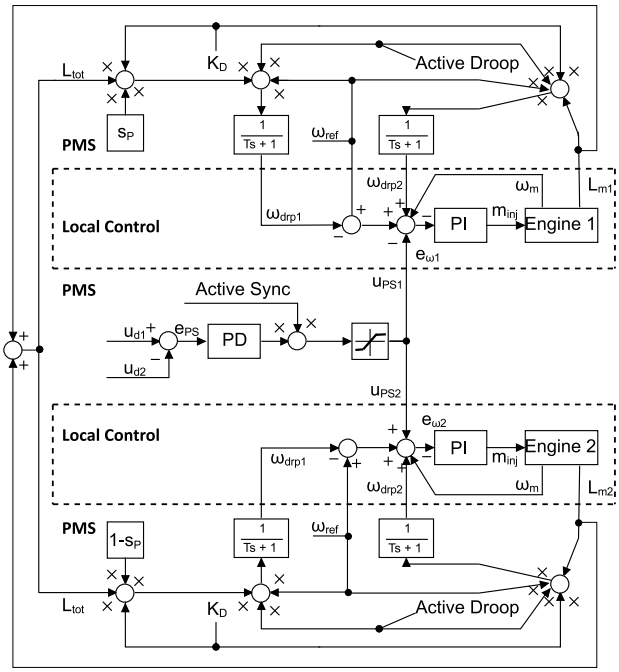

Figure 10: Engine speed control, active power sharing and phase synchronization for two gensets

3.3. Causality- and Simulation Control

When using hybrid models, it is important to have a *simulation controller*. In general, a simulation controller is not a controller using common sense, but rather a set of logic functions that controls the switching of the hybrid models. In this study, such a simulation controller would typically open and close circuit breakers, switch causality in the hybrid generator models and the resulting causality in the power grid. Functionality that restricts the input signals is also a common practice to implement, such as the generator setting the power grid voltage, which cannot be disconnected before model switching is performed.

The logic functions in the simulation controller are closely coupled to global controllers such as the phase synchronization controller and power sharing controller. The logics activate and deactivate these controllers, thereby ensuring that the integrators are

reset in addition to evaluating the controller performances, e.g. evaluating when the phase difference between the generators is small enough to close the circuit breaker. These functions are related to the functionalities found in real power management systems and in general it is up to the modeller or the PMS vendor to decide which functionality to implement, and is usually kept secret. In this paper, the PMS includes the functionalities needed to control the hybrid generator models, the circuit breakers and the power grid causality, and is functionally related to the phase synchronization control and power sharing control.

In particular, the PMS decides when to close the circuit when two generators are being synchronized. Here, a set of rules for closing the circuit when two generators are being synchronized, mainly based on minimizing numerical distortions when closing the circuit breakers, are implemented and given as

$$\begin{aligned} |\phi| &\leq \phi_{max} \\ |\frac{d\phi}{dt}| &\leq \dot{\phi}_{max} \\ |V_{rms,1} - V_{rms,2}| &\leq dV_{rms,max} \\ |f_{G,1} - f_{G,2}| &\leq df_{G,max} \end{aligned} \tag{49}$$

where ϕ_{max} is the maximal allowed phase difference, $\dot{\phi}_{max}$ is the maximal allowed derivative of the phase difference, $dV_{rms,max}$ is the maximal allowed difference in rms voltage between the two generators and $df_{G,max}$ is the maximal allowed difference in frequency between the two generators.

3.4. Overview of Control Structure

The control systems presented in this section are independent of the causality orientation of the generator model. This is shown in Figure 11 which shows a more coarser presentation of the control system structure and the connections between the PMS and the genset. The figure also shows that only the AVR and the engine speed controller, the governor, are always active, when neglecting the causality controller, while synchronization, active- and reactive load sharing are activated by the PMS when more than one generator is considered. Also note that the synchronization controller and the active load sharing adds to the reference signal for the engine speed controller, while the reactive load sharing adds to the output of the AVR. Note that the block i/u in the figure denotes the two causality models of the generator including the auxiliary engine.

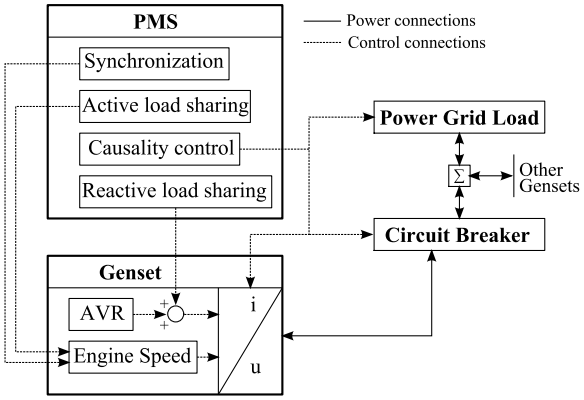

Figure 11: Control structure and connection between PMS and genset. Note that measurement signals needed by the PMS have been left out in the figure

4. Simulation

To test the hybrid generator model and the corresponding control systems, a simulation of the power plant given in Figure 2 is to be performed. Before presenting the simulation scenario and the corresponding simulation results, the parameters to be used in the simulation are presented.

4.1. Hybrid Genset Models and Power Grid Load

The generators are modeled as specified in section 2 and are assumed to be of equal size in this case study, having a rated power output of 2438 kW with $V_{rms} = 690\,\text{V}$ and $I_{rms} = 2010\,\text{A}$. The specific generator parameters are given in Table 5 in the Appendix and the time constant in the transfer function given in (13) is set to 0.001 s.

The specific fuel consumption for the auxiliary engines $b_e(P_e)$ is given as a polynomial,

$$b_e(P_e) = p_0 \left(\frac{P_e}{P_{e,max}}\right)^2 + p_1 \frac{P_e}{P_{e,max}} + p_2 \tag{50}$$

Table 2: Main parameters regarding the auxiliary engine models

Parameter	Value
$P_{e,max}$	2010 kW
J_m	$750\,kgm^2$
J_G	$750\,kgm^2$
b_f	$20\,{}^{kgm^2}/_{\mathrm{s}}$
n	$0.1-$
b_b	$\begin{cases} 0\,, & \text{if } m_f > 0 \\ 200\,, & \text{else} \end{cases}$
p_0	$56\,{}^{\mathrm{g}}/_{\mathrm{kWh}}$
p_1	$-70.8\,{}^{\mathrm{g}}/_{\mathrm{kWh}}$
p_2	$207\,{}^{\mathrm{g}}/_{\mathrm{kWh}}$

Table 3: Power grid load parameters and open circuit load parameter used in the simulation

Parameter	Value
Active power load	1 MW
Reactive power load	1 MVAr
Low-pass filter time constant	0.001 s
Open circuit load	100 MΩ

Table 2 list the parameters for the auxiliary engines used in the simulation.

The main parameters for the power grid load and the circuit breakers used in the simulation are given in Table 3. In addition to the constant active- and reactive power loads, biases and noise are added in order to make the simulation more realistic and to test the robustness of the total control system.

4.2. Control Systems

The control systems are implemented as specified in section 3 and the parameters are given in Table 4. Note that the control structure and the connections between the PMS and the gensets are as illustrated in Figure 11.

4.3. Simulation Scenarios

The simulation to be performed is designed to test the different control systems outlined in section 3 as well as the hybrid generator model and its real-time characteristics.

Table 4: Control parameters used in the simulation

Controller	Parameter	Value
AVR	V_{ref}	690 V
	K_p^{AVR}	5.0 -
	T_i^{AVR}	5.0 s
	Staturation	± 100.0 V
Reactive	S_{Qi}	0.5 - initially
Power	K_p^Q	1.0e-5 ${}^{\mathrm{V}}/_{\mathrm{VAr}}$
Sharing	T_i^Q	1.0 s
Engine	ω_{ref} (idle)	$20\ \pi\ {}^{\mathrm{rad}}/_{\mathrm{s}}$
Control	ω_{ref} (active)	$24\pi\ {}^{\mathrm{rad}}/_{\mathrm{s}}$
	K_p^ω	$0.1\ {}^{\mathrm{kgs}}/_{\mathrm{rad}}$
	T_i^ω	0.1 s
	Saturation	$[0, 0.26]$ kg
Synchronization	K_p^{PS}	$0.01\ {}^{\mathrm{rad}}/_{\mathrm{Vs}}$
Control	N_d^{PS}	10.0 -
	T_d^{PS}	0.008 s
Active	K_d	0.001 -
Power	S_{Pi}	0.5 - initially
Sharing	T_{LP}	0.01 s
PMS	ϕ_{max}	0.01 rad
	$\dot{\phi}_{max}$	$0.1\ {}^{\mathrm{rad}}/_{\mathrm{s}}$
	$dV_{rms,max}$	0.1 V
	$df_{G,max}$	$\frac{0.025}{\pi}$ Hz

In the simulation the two auxiliary engines driving the generators are started in the beginning of the simulation and given the idle speed reference. At $t = 20$ s, genset 1 is initiated, the engine gets the nominal speed reference and the AVR is fed the rms voltage reference. The circuit breaker that connects genset 1 to the power grid is closed at $t = 80$ s. Genset 2 is initiated at $t = 200$ s, in the same manner as genset 1, and the phase synchronization is activated. When the phase difference between the gensets is within the tolerance, the circuit breaker that connects genset 2 to the power grid is closed, and the model causality

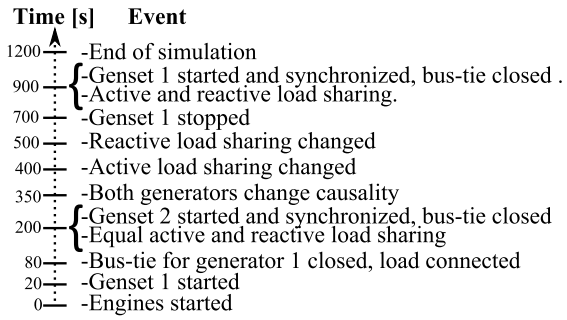

Figure 12: Simulation events

is changed from voltage to current. At $t = 350\,\mathrm{s}$, both gensets change causality; while genset 2 sets the power grid voltage. The active- and reactive power sharing are then changed at $t = 400\,\mathrm{s}$ and $t = 500\,\mathrm{s}$, respectively. In the end, genset 1 is stopped at $t = 700\,\mathrm{s}$ and started again at $t = 900\,\mathrm{s}$, and the active- and reactive load sharing are initiated with the last known sharing parameters, S_P and S_Q. A summary of all the simulation events is shown in Figure 12.

The Euler integration method is chosen as the solver with a solver time step $\Delta t = 0.0001\,\mathrm{s}$. The time step is chosen smaller than what was stated earlier; this due to an increase in the quality of the alternating voltages and currents results.

4.4. Simulation Results

The rms voltages calculated from (28) for the two generators are shown in Figure 13. The first plot shows the two generator rms voltages compared to each other. As can be seen in the plot, the voltages both converge to $690\,V$, when the gensets are active. As illustrated in Figure 12, genset 1 is first started and connected to the power grid load before genset 2 is started and synchronized to the power grid at $t = 200\,s$. At $t = 500\,s$, the causality of the two gensets is altered before genset 1 is disconnected from the power grid. In the end, genset 1 is reconnected to the power grid at $t = 900\,s$. The plot in the lower left-hand corner shows a closer view of what happens with the rms voltage for generator 1, which has output voltage causality when the load and the second generator are connected. When the power grid load

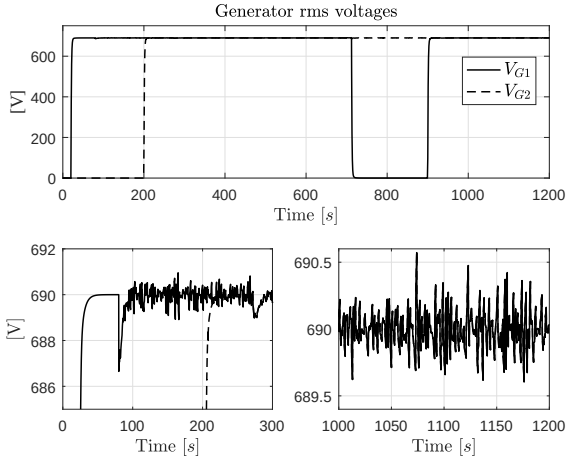

Figure 13: Generator rms voltages

is connected, the rms voltage for generator 1 gets a small dip before being controlled back to its reference. The dip has a magnitude of approximately $3\,\mathrm{V}$ which results in a change in rms voltage of approximately $0.43\,\%$, which is well within any typical realistic tolerance, typically $\sim 1\,\%$ of the reference rms voltage. A small dip in the rms voltage can also be seen when the second generator is connected, which is expected to be due to the stabilization of the two connected generators, and due to the start of the load-sharing procedure. However, this dip is smaller, having a magnitude of $0.5\,V$, approximately $0.072\,\%$ of the rms reference voltage. The last plot in the lower right-hand corner shows the rms voltage fluctuations in the time range $t \in [1000\,\mathrm{s}, 1200\,\mathrm{s}]$. As can be seen, the rms voltages for the two generators overlap, although some noise is present. This noise is due to the noise added in the power grid load in order to test the robustness of the power plant. The noise magnitude is quite low, at the most approximately $0.1304\,\%$ of the rms voltage reference, but large enough to indicate stability and robustness in the total power plant model.

Figure 14 shows the two generator frequencies compared to each other. The first plot shows the comparison of the two generator frequencies during the entire

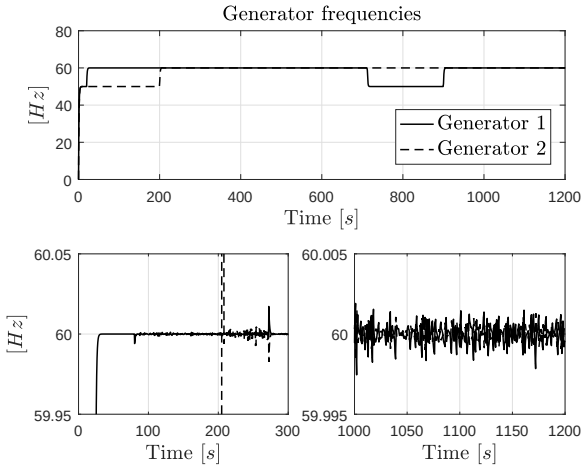

Figure 14: Generator frequencies

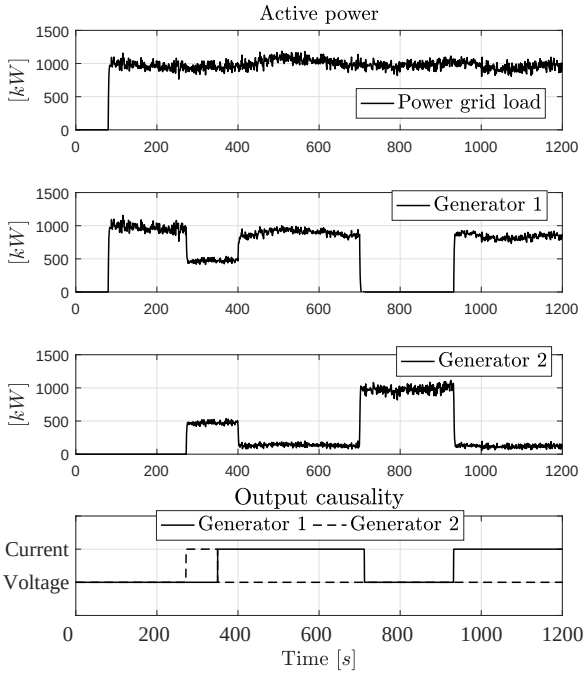

Figure 15: Active Power

simulation, and the characteristics are comparable to the rms voltage characteristics in the first plot in Figure 13, except that when a generator is disconnected from the power grid, it runs in an open circuit at an idling speed of 600 rpm. The plot given in the lower left-hand corner shows a closer view of the frequencies at the start of the simulation. The characteristic dip when the load is connected is also present here, having a magnitude of approximately 0.06 Hz. When the second genset is started, the frequency of generator 2 overshoots the first generator frequency, due to phase synchronization, with a magnitude of approximately 0.08 Hz before converging to the desired frequency. When the two generators are connected the active power sharing characteristics can be seen at approximately $t = 272\,s$. Genset 1 increases its frequency, whereas genset 2 slows down due to the droop control. Nonetheless, these frequency peaks are quite small, approximately 0.02 Hz. The last plot, given in the lower right-hand corner of the figure, shows the frequency fluctuations due to the noise. Note that the two generator frequencies do not overlap as the rms voltages do in Figure 13, which is expected due to the noise and the active power sharing control.

The active power production and consumption are shown in Figure 15, in addition to the genset output causalities. The first plot in the figure shows the active power grid load, which oscillates at around 1 MW with a relatively high frequent noise, having a maximal amplitude of 150 kW and a maximal frequency of 0.5 Hz, in addition to a slowly varying oscillating bias, modeled as being integral to white noise. The plot also shows that the load is increased relatively quickly; when connected, it takes approximately 5 s from when the load is connected until it reaches its full potential of power consumption. The second and third plot show the active power generated by genset 1 and 2, respectively. From the two plots, it can be seen that the noise experienced by the gensets decreases when both gensets are active due to active load sharing. One can also see that the sum of generated active power equals the active power consumed by the power grid load. The last plot shows the output causality of the two gensets. Note that before

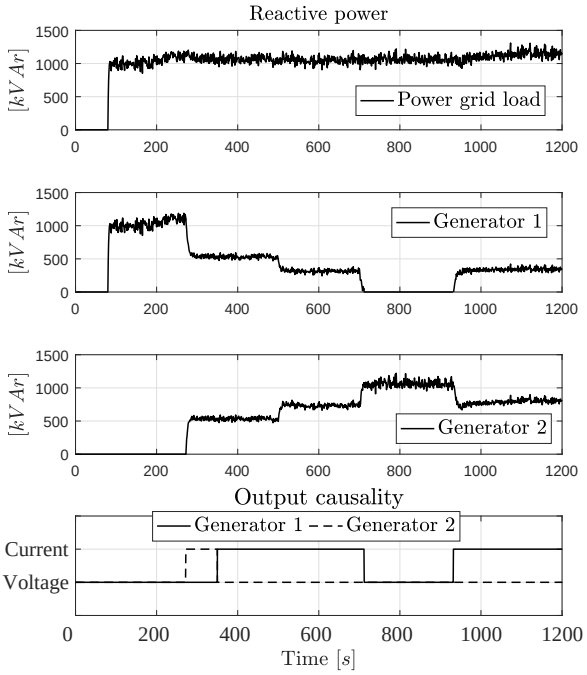

Figure 16: Reactive Power

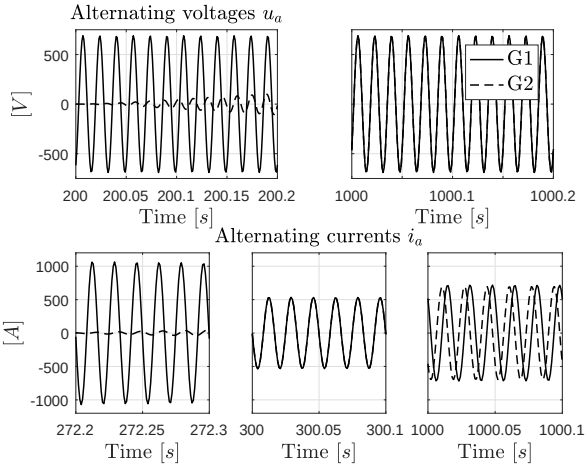

Figure 17: Voltages and currents, a, in the (a, b, c)-reference frame

genset 1 is stopped all the active power production is transferred to genset 2. This is one of the many functionalities implemented in the PMS.

Figure 16 shows the reactive power for the two gensets and the power grid load, as well as the genset output causalities. As can be seen in the figure, the results are similar to the ones presented in Figure 15, the sum of the reactive power for the two gensets equals the reactive power in the power grid load, and that all the reactive power is transferred to genset 2 before genset 1 is stopped.

Figure 17 shows the alternating voltages u_a and currents i_a for the two generators in the chosen time ranges. The plot in the upper left-hand corner shows the u_a for the two generators when genset 2 is started, while the upper plot to the right shows the two voltages in a time range when both circuit breakers are closed. When both generators are connected to the grid, the alternating voltages should overlap, which the upper right-hand plot proves. The plot in the lower left-hand corner shows the currents i_a right after genset 2 is connected, and the reactive load sharing controller has just been activated. This can be seen in the end of the plot, in which the current form genset 2 is starting to increase. The lower plot in the middle shows the two currents in an equal reactive power sharing settings, and the last plot shows a time range when the reactive power sharing is asymmetric.

4.5. System Evaluation

The simulation results show that the hybrid generator models seem to be stable, which is not that surprising according to the chosen solver time step. Also, the results show that switching between causalities do not affect the simulation results. This means that the integrator reset algorithm and the inheritance of initial conditions are done correctly in the model.

The control systems also seem to work properly, being able to both control the power grid frequency, the power grid rms voltage, phase synchronization and load sharing in a fast and stable manner despite being simple PID-based control laws. Such control

laws are also used widely in the industry because they are simple to implement, simple to tune and quite robust as long as the controlled systems have strong linear characteristics in the controlled region or certain passivity properties.

The total simulation of 1200 s was solved in approximately 100 s, giving a solving speed of approximately 12 times real-time. This indicates that the computational efficiency is being maintained for real-time application purposes without affecting the quality of the simulation results.

5. Conclusion

This paper set out to present a generic framework for modeling and simulating marine power plants with weak power grids in transient operations. The generator model presented in this work is a hybrid model that has the ability to switch between outputs and inputs, which makes it suited for transient power plant operations such as genset start-up and shutdown, as well as phase synchronization control. This also enables the ability to test failure modes such as genset trippings due to the overload or overstepping of power grid frequency tolerances, but which has not been discussed in any detail in this paper.

Two hybrid causality generator models were implemented in a small marine power plant as a case study. The differential causality in the voltage output generator model was solved by differentiation using a transfer function, and a generator parameter analysis was conducted based on the system eigenvalues. The current output model seemed to be difficult to solve using simple integration methods such as the Euler method, but a simulation setup that enabled the use of the Euler method in a larger scale simulation, such as the one performed, was proposed and tested through simulations.

An overall power plant control was proposed through the control of the field voltages and the engine speeds by using simple but effective controllers for rms voltage, engine speed, phase synchronization and active- and reactive power sharing. The simulation results demonstrated that the total power plant model was stable, even though noise was added, and all transient effects of interest could be reflected through the simulation results. The results also demonstrated the equivalence between the $(d, q, 0)$-reference frame and the (a, b, c)-reference through comparison with well-known alternating generator characteristics. The simulation results are also comparable to the results obtained in [18], in which the simulation results were verified with experimental data. Also, the power plant itself showed good real-time conditions, being solved about 12 times faster than real-time.

In further work, the proposed power plant framework should be validated against experimental results. However, since the genset models are based on well-known equations, it is believed that the simulation results should converge to experimental results, as long as enough information about the control laws and the power management system is given. Also, a sophisticated outer control law for planning the total power plant operation, e.g. deciding when to start and stop a genset from power plant measurements, should be considered. This is out of scope here but it is believed that the power plant model presented in this case study gives a good foundations for such studies.

Acknowledgements

Thanks to all parties engaged in the *ViProMa*-project, Virtual Prototyping of Marine systems and operations, for supporting and financing the research topics this paper presents.

References

[1] R. Nilsen, I. Sorfonn, Hybrid Power Generation Systems, in: 2009 13th European Conference on Power Electronics and Applications, 2009, pp. 1–9.

[2] E. K. Dedes, D. A. Hudson, S. R. Turnock, Assessing the potential of hybrid energy technology to reduce exhaust emissions from global shipping, Energy Policy 40 (2012) 204–218.

[3] S. Skjong, E. Pedersen, Non-angular MPC-based Thrust Allocation Algorithm for Marine Vessels - A Study of Optimal Thruster Commands,

IEEE Transactions on Transportation Electrification (2017) 1–1.

[4] M. Morsy El-Gohary, Overview of past, present and future marine power plants, Journal of Marine Science and Application 12 (2) (2013) 219–227.

[5] D. Sahm, A two-axis, bond graph model of the dynamics of synchronous electrical machines, Journal of the Franklin Institute.

[6] T. A. Pedersen, E. Pedersen, Bond graph modelling of marine power systems, Mathematical and Computer Modelling of Dynamical Systems.

[7] J. Machowski, J. W. Bialek, J. R. Bumby, Power system dynamics: stability and control, 2nd Edition, Chichester, U.K. Wiley, 2008.

[8] A. Davoudi, L. Qu, P. L. Chapman, Summary of Recent Work on Reduction Techniques Applied to Electromechanical Modeling, in: 2007 IEEE Electric Ship Technologies Symposium, IEEE, 2007, pp. 363–370.

[9] A. Davoudi, Reduced-order Modeling of Power Electronics Components and Systems, University of Illinois, 2010.

[10] J. Cathey, R. Cavin, A. Ayoub, Transient Load Model of an Induction Motor, IEEE Transactions on Power Apparatus and Systems PAS-92 (4) (1973) 1399–1406.

[11] D. P. Carroll, P. Krause, Stability Analysis of a DC Power System, IEEE Transactions on Power Apparatus and Systems PAS-89 (6) (1970) 1112–1119.

[12] C. Cho, J.-H. Jeon, J.-Y. Kim, S. Kwon, K. Park, S. Kim, Active Synchronizing Control of a Microgrid, IEEE Transactions on Power Electronics 26 (12) (2011) 3707–3719.

[13] M. N. Marwali, J.-W. Jung, A. Keyhani, Control of distributed generation systems - Part II: Load sharing control, IEEE Transactions on Power Electronics 19 (6) (2004) 1551–1561.

[14] D. C. Karnopp, D. L. Margolis, R. C. Rosenberg, System Dynamics: Modeling and Simulation of Mechatronic Systems, John Wiley & Sons, Inc., New York, NY, USA, 2006.

[15] K. Edström, Switched Bond Graphs: Simulation and Analysis, Ph.D. thesis, Linköping University, Automatic Control (1999).

[16] P. J. Mosterman, G. Biswas, A theory of discontinuities in physical system models, Journal of the Franklin Institute.

[17] C. D. Beers, E.-J. Manders, G. Biswas, P. J. Mosterman, Building efficient simulations from hybrid bond graph models, 2006.

[18] T. A. Pedersen, Bond Graph Modeling of Marine Power Systems, Ph.D. thesis, Norwegian University of Science and Technology, Department of Marine Technology (2009).

[19] B. Rokseth, S. Skjong, E. Pedersen, Modeling of Generic Offshore Vessel in Crane Operations With Focus on Strong Rigid Body Connections, IEEE Journal of Oceanic Engineering PP (99) (2016) 1–23.

[20] S. Skjong, E. Pedersen, Co-Simulation of a Marine Offshore Vessel in DP-Operations including Hardware-In-the-Loop (HIL), in: Proceedings of the ASME 2017 36th International Conference on Ocean, Offshore, and Arctic Engineering OMAE 2017, Trondheim, Norway, 2017.

[21] P. C. Krause, C. H. Thomas, Simulation of Symmetrical Induction Machinery, IEEE Transactions on Power Apparatus and Systems 84 (11) (1965) 1038–1053.

[22] A. C. Umarikar, L. Umanand, Modelling of switching systems in bond graphs using the concept of switched power junctions, Journal of the Franklin Institute.

[23] U. M. Ascher, L. R. Petzold, Computer Methods for Ordinary Differential Equations and Differential-Algebraic Equations, Statewide Agricultural Land Use Baseline 2015 1 (1998) 332.

[24] J. Belanger, P. Venne, J.-N. Paquin, The What, Where and Why of Real-Time Simulation, Planet RT 1 (0) (2010) 37–49.

[25] C.-T. Chen, Linear System Theory and Design, 3rd Edition, Oxford University Press, Inc., New York, NY, USA, 1998.

[26] J. B. Heywood, Internal Combustion Engine Fundamentals, Automotive technology series, McGraw-Hill, 1988.

[27] J.-P. Steghöfer, G. Anders, F. Siefert, W. Reif, A System of Systems Approach to the Evolutionary Transformation of Power Management Systems., in: GI-Jahrestagung, 2013, pp. 1500–1515.

[28] J. P. Louis, Control of Synchronous Motors, ISTE, Wiley, 2013.

[29] S. Funabiki, A. Hitsumoto, Y. Yamakawa, T. Ito, Automatic voltage regulation of synchronous generator with pole assignment self-tuning regulator, in: Industrial Electronics, Control and Instrumentation, 1991. Proceedings. IECON '91., 1991 International Conference on, 1991, pp. 1807–1811 vol.3.

[30] K. J. Astrom, L. Rundqwist, Integrator Windup and How to Avoid It, in: 1989 American Control Conference, 1989, pp. 1693–1698.

[31] Y. Han, H. Li, P. Shen, E. A. A. Coelho, J. M. Guerrero, Review of Active and Reactive Power Sharing Strategies in Hierarchical Controlled Microgrids, IEEE Transactions on Power Electronics 32 (3) (2017) 2427–2451.

[32] D. J. McGowan, D. J. Morrow, B. Fox, Integrated governor control for a diesel-generating set, IEEE Transactions on Energy Conversion 21 (2) (2006) 476–483.

6. Appendix

The generator used in this paper has a rated power output of 2438 kW with $V_{rms} = 690\,\mathrm{V}$ and $I_{rms} = 2010\,\mathrm{A}$. The specific parameters used are given in Table 5.

Table 5: Generator parameters

Parameter	**Value**	**Parameter**	**Value**
L_d	0.0007728 H	L_{qQ}	0.0104431 H
L_D	0.5987330 H	n_p	5 –
L_f	0.6063750 H	R_d	0.0049700 Ω
L_{dD}	0.0162176 H	R_D	6.2165657 Ω
L_{df}	0.0162176 H	R_q	0.0049700 Ω
L_{fD}	0.5769750 H	R_Q	9.7575356 Ω
L_q	0.0005257 H	R_f	0.3150000 Ω
L_Q	0.3987454 H	f_G	60 Hz